

See discussions, stats, and author profiles for this publication at: <https://www.researchgate.net/publication/232718189>

Water Structure, Dynamics, and Spectral Signatures: Changes Upon Model Cavity–Ligand Recognition

ARTICLE *in* THE JOURNAL OF PHYSICAL CHEMISTRY B · OCTOBER 2012

Impact Factor: 3.3 · DOI: 10.1021/jp309373q · Source: PubMed

CITATIONS

5

READS

27

3 AUTHORS, INCLUDING:



Riccardo Baron

Baron Research Group, New York, United States

62 PUBLICATIONS 2,267 CITATIONS

[SEE PROFILE](#)



Francesco Paesani

University of California, San Diego

92 PUBLICATIONS 2,354 CITATIONS

[SEE PROFILE](#)

Water Structure, Dynamics, and Spectral Signatures: Changes Upon Model Cavity–Ligand Recognition

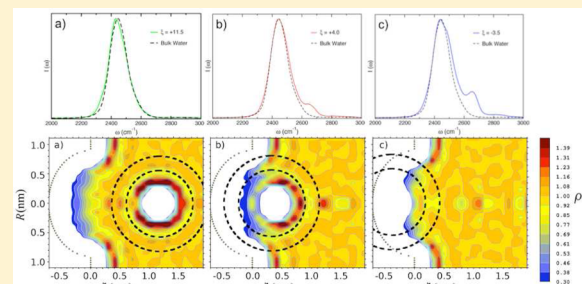
Riccardo Baron,*||,†,‡ Piotr Setny,*§ and Francesco Paesani*,†

†Department of Chemistry and Biochemistry, University of California, San Diego, La Jolla, California 92093, United States

‡Center for Theoretical Biological Physics, University of California, San Diego, La Jolla, California 92093, United States

§Physics Department T38, Technical University Munich, James Franck Str. 1, 85748 Garching, Germany

ABSTRACT: It is becoming increasingly evident that water plays an active role in noncovalent receptor–ligand association. In this study, hydrophobic cavity–ligand association in a model system is characterized through the analysis of the structure, dynamics, and corresponding spectral signatures of water at different stages of the binding process. Molecular dynamics simulations reveal that the reorientation of the water molecules around the ligand becomes faster as the receptor–ligand distance reduces, which is correlated with the decrease in number of water–water hydrogen bonds within the ligand hydration shells. Prompted by the need for calculating physical quantities that can be amenable to experimental validation, the changes in the spectroscopic features upon cavity–ligand binding are investigated. The analysis of both linear and nonlinear infrared spectra allows direct insight into the evolution of water structure and dynamics around the ligand. In particular, characteristic spectroscopic features emerge at key stages of the binding process, which are related to changes in the hydrogen-bond topology of water around the ligand. This study demonstrates that computer simulations and vibrational spectroscopy could be integrated to facilitate the direct study of solvent effects in biomolecular association.



1. INTRODUCTION

The role of molecular recognition in chemistry cannot be overemphasized. Recent molecular dynamics (MD) simulation studies of model systems show that cavity–ligand association can be driven by overall-dominating water-related contributions. In contrast to the dominant view of the solvent as a passive, embedding medium for molecular association processes, water appears to be an active player in noncovalent molecular binding.^{1–4} The counterintuitive observation that water-related contributions (e.g., ligand dehydration and creation of water–water interactions) may dominate over the direct ligand–cavity interaction has broad implications for understanding virtually all molecular association processes occurring in solution and is expected to be transferable to biologically relevant scenarios. For example, it is most crucial for the interpretation of biophysical experiments,^{5,6} the development of protein–ligand binding theory,^{3,4} and computational approaches to predict drug-binding affinities.^{7–9}

A chief obstacle to directly probe the link among water structure, dynamics, and thermodynamics is the dependence of water-related effects on the subtle reorganization of water at diverse length and time scales. Although the comparison between computed and measured thermodynamic properties is possible for molecular liquids (e.g., the thermodynamics of hydrogen bonding¹⁰), there is still a clear gap between simulations and experimental observations in the case of molecular association thermodynamics. This gap is particularly relevant from the viewpoint of experiment interpretation

because sophisticated techniques are needed to directly probe changes of water structure and dynamics upon binding, and disentangle their contributions from the dominating background of bulk solvent.⁷ Therefore, the investigation of more treatable model systems is preferable from theoretical and computational viewpoints.^{1,2,11–20}

A noticeable impact of changes in water structure and dynamics on the thermodynamic outcome of a binding process have been demonstrated in recent simulations of model receptor–ligand systems.^{1,2} In the case of purely apolar system, with receptor cavity of 0.8 nm radius² considered also in the current study, the association occurred to be driven by enthalpy and opposed by entropy, contrary to the common view of entropy-dominated hydrophobic interactions. Such a peculiar thermodynamic signature was an effect of the suppression of solvent fluctuations (highly entropic) in the weakly hydrated cavity binding region and favorable enthalpy gain resulting from the formation of more numerous, geometrically optimal, and energetically favorable water–water interactions by the released solvent molecules.^{1,2,7} Cavity hydration can be altered by changing its radius: in line with the capillarity theory,²¹ larger cavities are expected to remain preferably wet, while smaller cavities are preferably dry. Indeed, the latter notion was confirmed by explicit solvent MD studies of analogous

Received: September 21, 2012

Revised: October 27, 2012



receptor–ligand system, in which receptor cavity of 0.5 nm radius remained dewetted.¹²

The importance of water-related thermodynamic contributions described for purely apolar cavity–ligand binding is likely transferable to partly hydrophilic cavities typically found in complex biomolecular receptors.²² In this case, localization or delocalization of water molecules upon binding can be favorable or unfavorable depending on (i) the number of water molecules that preoccupy the hydratable regions of the binding site considered²² and (ii) seemingly subtle differences in the surrounding physicochemical environment that determine how mobile these water molecules are in the unbound state vs bulk. These alternative scenarios have nontrivial effects on ligand binding because water (de)localization can be a major source of ligand-binding free energy.^{8,9,23–27} In this context, the ability to obtain and characterize spectroscopic features corresponding to the relevant water behavior could greatly improve the interpretation of experimental data on binding thermodynamics.

One current focus of experiments on solvation dynamics is to directly probe fast-time scale events without changing the equilibrium behavior of the system under study. In this context, ultrafast vibrational spectroscopy has emerged in the last years as a powerful tool for studying the structure and dynamics of liquid water in different environments.^{28–30}

In this study, the link between water dynamics and structure in cavity–ligand association is investigated together with the evolution of the associated spectroscopic signatures to address three fundamental questions of general relevance in ligand binding processes: How do water structural and dynamic properties change at key stages along the binding coordinate? Are these properties reflected in changes of the associated IR spectral features? Can simulations and vibrational spectra calculation enable the development of integrated experimental/computational approaches to capture the microscopic picture of water dynamics and its thermodynamic implications?

2. COMPUTATIONAL METHODOLOGY

All classical MD simulations were carried out on a larger version of the Setny's cavity model described in refs 1, 2, 12, and 13. Specifically, the studied system consists of one hemispherical cavity of 0.8 nm radius embedded in a rectangular paraffin-like wall of dimension 3.5×3.3 nm, composed of 4242 (positionally constrained) particles, aligned in a hexagonal close packed (HCP) lattice (Figure 1). The parameters of the wall-water Lennard-Jones potential are tuned to represent a paraffin-like material. The system is filled with

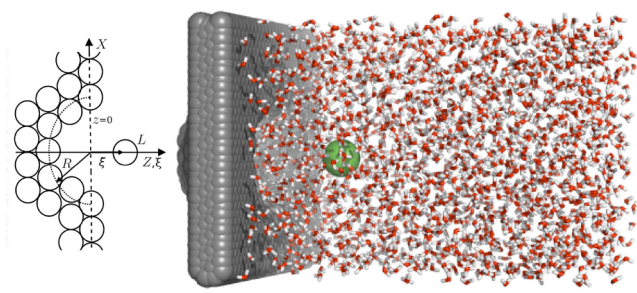


Figure 1. Schematic representation and snapshot of the apolar cavity–ligand system studied. The hydrophobic hemispherical cavity (radius, $R = 0.8$ nm, gray) and hydrophobic ligand (L , green) are highlighted. Note that $\xi = 0.0$ nm corresponds to the wall surface.

1950 TIP4P water molecules,³¹ resulting in a box with edge $z \approx 5.4$ nm from the cavity wall. The apolar ligand is modeled as one LJ sphere with OPLS methane parameters.³² The system used in this study is identical to that previously described in ref 33 for atomic-level simulations. The hemispherical paraffin wall and cavity include 4242 (positionally constrained) particles. The reaction coordinate ξ used to describe the cavity–ligand binding process represents the distance between the ligand center and the plane of the cavity wall surface ($\xi = 0$; Figure 1) and corresponds to the symmetry axis of the simulation box. For $\xi < 0$, the ligand is considered inside the cavity. To avoid dependence of the atomic fluctuations, and hence the spectra on thermostat algorithms, all simulations were performed in the microcanonical (NVE) ensemble with CHARMM³⁴ integrating Newton's equations of motion with a time step of 1 fs. We note that NVE simulations were required for the analysis of the hydrogen-bond dynamics and calculations of the infrared spectra from the relevant time-correlation functions. Periods of 2 ns were used for the analysis. The SHAKE algorithm³⁵ was used to keep TIP4P water molecules rigid during the simulations. The position of the methane ligand was kept on the reaction coordinate and at desired distances from the cavity wall through a restraining potential with a force constant of 100 kcal/mol Å².

The rotational dynamics of the water molecules around the ligand at different positions along the reaction coordinate was studied in connection with the associated vibrational spectroscopic signatures. For analysis, only the water molecules residing within $r = 0.55$ nm or $r = 0.8$ nm of the ligand were considered, which approximately correspond to one and two ligand solvation shells around in bulk water. To make a direct connection with recent experimental and theoretical studies of linear and nonlinear spectra, we modeled our system as a dilute mixture of HOD in H₂O (which hereafter will be referred to as the HOD:H₂O system). Specifically, each of the selected water molecules was considered in turn as a HOD molecule by replacing one of the H atoms with a D atom. Linear and nonlinear IR spectra for the HOD molecules were computed according to a well-established mixed quantum-classical (QC) scheme.³⁶ Specifically, the OD spectral line, $I(\omega)$, corresponding to the 1–0 vibrational transition of the effective HOD molecules was calculated as

$$I(\omega) = \frac{1}{2\pi} \int_{-\infty}^{+\infty} dt e^{-i\omega t} \times \langle \mu_{10}(0) \cdot \mu_{10}(t) \exp[i \int_0^t d\tau \omega_{10}(\tau)] \rangle \quad (1)$$

where $\mu_{10}(t)$ and $\omega_{10}(t)$ are, respectively, the vibrational transition moment and the vibrational frequency associated to the transition between the ground and excited state of the OD stretch at time t , and the brackets denote a classical equilibrium average. The nonlinear 2D-IR signal, $I(\omega_1, t_2, \omega_3)$, was calculated from the double Fourier–Laplace transforms over t_1 and t_3 of the rephasing, $R_r(t_3, t_2, t_1)$, and nonrephasing, $R_{nr}(t_3, t_2, t_1)$, third-order response function including non-Condon effects:³⁶

$$I(\omega_1, t_2, \omega_3) \equiv \text{Re} \int_0^\infty dt_1 \times \int_0^\infty dt_3 [e^{i(-\omega_1 t_1 + \omega_3 t_3)} R_r(t_3, t_2, t_1) + e^{i(\omega_1 t_1 + \omega_3 t_3)} R_{nr}(t_3, t_2, t_1)] \quad (2)$$

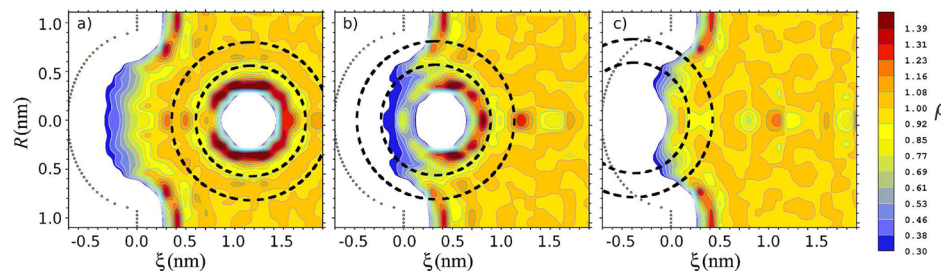


Figure 2. Key steps along the cavity–ligand binding coordinate, ξ . Water density maps normalized to the bulk ($\rho = 1$) are shown for snapshots with the ligand in the water bulk (a, $\xi = 1.15$ nm), in an intermediate state at which cavity dewetting begins (b, $\xi = 0.40$ nm), and in the bound state (c, $\xi = -0.35$ nm). Black circles of 0.55 and 0.8 nm radii indicate solvent regions considered for obtaining spectroscopic data.

Within the QC framework, the instantaneous OD frequencies were computed for all the molecular configurations extracted from the MD trajectories by solving the Schrödinger equation for the corresponding 1-dimensional OD oscillator using the Numerov method.³⁷ Following the procedure described in refs 38 and 39 for any given configuration, the underlying OD Born–Oppenheimer potential energy curve was computed by stretching the OD bond of the HOD molecule, while keeping the positions of all other atoms fixed (including both ligand and remaining water molecules). The resulting potential curve was then used to compute both the corresponding vibrational frequency and the vibrational wave functions of the ground and first excited states. The vibrational transition moments, $\mu_{10}(t)$, were calculated within the same computational scheme from the numerical integration over the product of the molecular dipole moment and the appropriate vibrational wave functions.⁴⁰ In solving the 1-dimensional Schrödinger equation, the ab initio-based and polarizable TTM3-F model⁴¹ was used to describe both the inter- and intramolecular interactions of the water molecules, while the water–ligand and water–wall interactions were still described in terms of the TIP4P-derived parameters. Previous studies have shown that the TTM3-F model provides an accurate description of the IR spectra of bulk water.^{38,40,41} The analysis of both rotational dynamics and spectroscopic features for each value of ξ was carried out over a continuous period of 200 ps extracted from the corresponding 2 ns simulation, which was found to be sufficient to obtain converged results.

3. RESULTS AND DISCUSSION

Water dynamics around the methane-like ligand was studied at three different positions along the reaction coordinate (Figure 2), corresponding to configurations with the ligand in the bulk ($\xi = 1.15$ nm), at the water surface ($\xi = 0.4$ nm), and inside the cavity ($\xi = -0.35$ nm). When the ligand is located in the bulk, the system is characterized by slow water fluctuations in and out of the cavity on the time scale of ~ 100 ps, as previously reported.¹² These fluctuations are suppressed upon binding ($\xi \leq 0.40$ nm) as the ligand dehydrates, and disordered water is expelled from the cavity, giving rise to unfavorable entropic contribution to binding Gibbs energy (ΔG).^{1,2} At $\xi \approx -0.35$ nm, ΔG reaches a minimum corresponding to molecular configurations with the ligand bound to the cavity.^{1,2}

Direct insights into water dynamics around the ligand at different stages of the binding process can be obtained from the orientational time autocorrelation function, $C_2(t)$. Here, $C_2(t) = \langle P_2[\mathbf{e}(0) \cdot \mathbf{e}(t)] \rangle$ is the time autocorrelation function of the second-order Legendre polynomial $P_2[\mathbf{e}(0) \cdot \mathbf{e}(t)]$, where $\mathbf{e}(t)$ is a unit vector that lies along one of the two O–H bonds of each

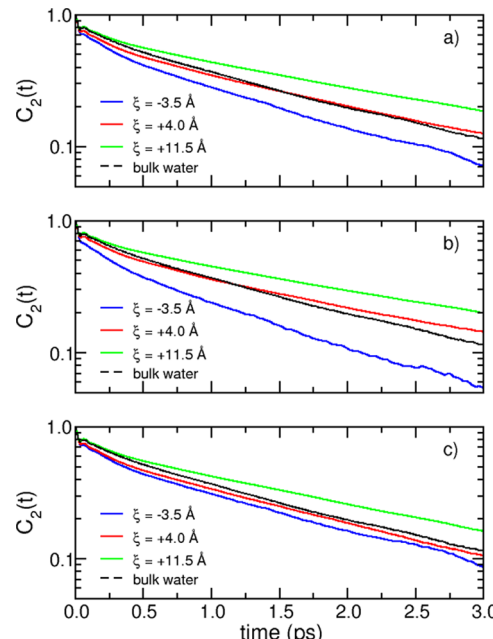


Figure 3. Orientational correlation functions, $C_2(t)$, calculated for molecules around the ligand at the key steps along the cavity–ligand coordinate, ξ , shown in Figure 1 (green, $\xi = 1.15$ nm; red, $\xi = 0.40$ nm; blue, $\xi = -0.35$ nm). $C_2(t)$ is shown for (a) all molecules within $r = 0.80$ nm of the ligand, (b) all molecules within $r = 0.55$ nm of the ligand, and (c) all molecules with $0.55 \text{ nm} \leq r \leq 0.80 \text{ nm}$. $C_2(t)$ for bulk (TIP4P) water is also shown (black dashed lines) for reference.

Table 1. Changes in Water Dynamics around the Ligand at Key Stages of the Molecular Recognition Process^a

ξ (nm)	τ_2 (ps) $r \leq 0.80$ nm	τ_2 (ps) $r \leq 0.55$ nm	τ_2 (ps) $0.55 \text{ nm} \leq r \leq 0.80 \text{ nm}$	τ_2 (ps) bulk
-0.35	1.4 ± 0.1	1.3 ± 0.1	1.6 ± 0.1	1.7
0.40	1.8 ± 0.1	2.0 ± 0.1	1.7 ± 0.1	1.7
1.15	2.3 ± 0.1	2.4 ± 0.1	2.1 ± 0.1	1.7

^aThe relaxation times (τ_2) associated with the decay of the orientational correlation function calculated for water molecules within different shells around the ligand (r) are reported as a function of the cavity–ligand distance (ξ). Corresponding values for bulk water are given as reference in the fifth column.

H_2O molecule. $C_2(t)$ is related to the anisotropy coefficient that can be measured in ultrafast vibrational pump–probe experiments.^{28,42} $C_2(t)$ calculated for water molecules within $r = 0.8$ nm of the ligand positioned at $\xi = 1.15$, 0.4, and 0.35 nm are shown in Figure 3, along with the corresponding reference curve calculated for bulk water. The associated relaxation times

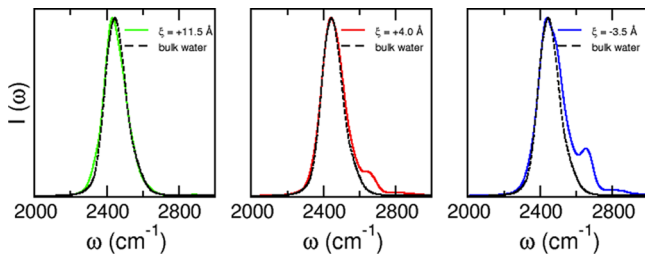


Figure 4. OD infrared lineshape, $I(\omega)$, calculated for molecules within $r = 0.80$ nm of the ligand at key stages along the cavity–ligand binding coordinate, ξ , shown in Figure 1 (green, $\xi = 1.15$ nm; red, $\xi = 0.40$ nm; blue, $\xi = -0.35$ nm).

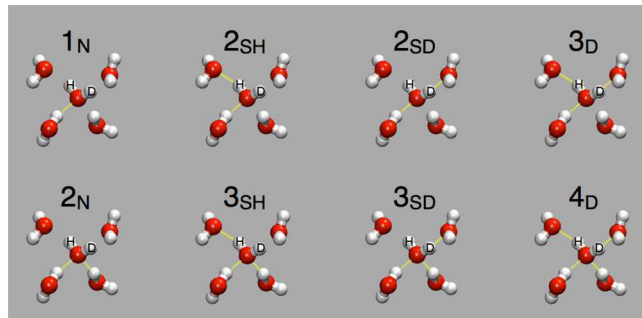


Figure 5. Hydrogen-bond topologies used to characterize the local structure of water around the ligand in connection with the corresponding infrared lineshapes.

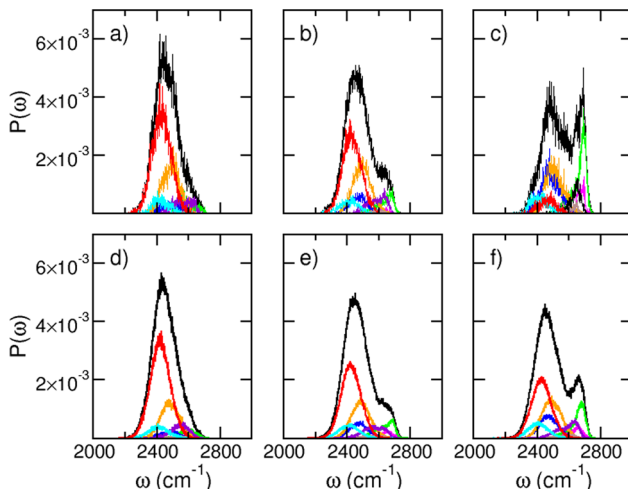


Figure 6. Normalized contributions to the infrared spectra signatures due to different water H-bond topologies calculated from molecular dynamics simulations at the key stages along the cavity–ligand binding coordinate, ξ , as in Figure 1. (a) $\xi = 1.15$ nm, (b) $\xi = 0.40$ nm, and (c) $\xi = -0.35$ nm. Each color line represents the individual contribution from the hydrogen-bond topologies shown in Figure 5. Top panels: contributions from water molecules within $r = 0.55$ nm of the ligand. Bottom panels: contributions from water molecules with $0.55 \text{ nm} \leq r \leq 0.80 \text{ nm}$. Note that the 4_{H} mode (red line) dominates in bulk, but its population decreases when water is disordered and assumes suboptimal geometries inside the hydrophobic cavity. Conversely, modes 2_{SD} and 2_{SH} (blue and green lines, respectively) display distributions increasingly visible when the ligand moves toward the cavity. The 3_{D} mode (orange line) remains essentially unaltered. The 3_{SH} and 3_{SD} modes are shown in violet and cyan, respectively. The modes 1_{N} (magenta) and 2_{N} (brown) are small in all cases.

(τ_2) obtained from exponential fits to the long-time decays of $C_2(t)$ are reported in Table 1. At $\xi = 1.15$ nm, the effects of the cavity–water interface on the hydration structure around the ligand can be considered negligible (Figure 1), and this configuration is effectively analogous to a small hydrophobe in bulk water. Consequently, as discussed in refs 43 and 44, the reorientation of the H_2O molecules around the ligand is slowed down relative to pure water. As the ligand approaches the cavity, the water orientational dynamics in the hydration shells becomes progressively faster with τ_2 at $\xi = -0.35$ nm being significantly smaller than the corresponding value calculated in pure water. These changes in water dynamics can be directly correlated with changes in the hydration structure along the binding coordinate. At $\xi = 0.40$ nm, Figure 2 shows that water around the ligand can be conveniently described in terms of two populations including molecules located on the left side (cavity side) and on the right side (bulk side). Although in this configuration the ligand is still fully hydrated, the presence of the cavity disrupts the interface leading to locally different water structures on the two sides. When the ligand–cavity distance is about $\xi = -0.35$ nm, only few water molecules (~ 4) are transiently found inside the cavity around the ligand. This implies that the H_2O molecules located within 0.8 nm of the ligand mainly belong to the top layers of the water interface on the right side of the ligand.^{12,33}

To better characterize the hydration dynamics as a function of the distance of the ligand from the cavity, $C_2(t)$ was also calculated for H_2O molecules located within $r = 0.55$ nm from the ligand, corresponding approximately to the first hydration shell at $\xi = 1.15$ nm. The results are summarized in Figure 3 and Table 1. For $\xi = 1.15$ nm and $\xi = 0.40$ nm, the reorientation of the water molecules in the first hydration shell is further slowed down relative to the bulk, while for $\xi = -0.35$ nm, the water reorientation becomes noticeably faster. In the latter case, the H_2O molecules that are within 0.55 nm of the ligand correspond to molecules that are either transiently located inside the cavity or belong to the topmost layer of the water surface. As a consequence, the H-bond topology and associated rotational dynamics of these H_2O molecules are significantly affected by the presence of both cavity and ligand. The change in behavior of the H_2O molecules around the ligand upon binding is clearly manifested by the initial drop of $C_2(t)$ that becomes more pronounced as ξ decreases. At $\xi = -0.35$ nm, the H_2O molecules around the ligand are not part of an extended H-bond network. Therefore, they can effectively reorient in the absence of restoring forces, which results in large librational motions responsible for the increased $C_2(t)$. The analysis of $C_2(t)$ for water molecules within $0.55 \text{ nm} \leq r \leq 0.8 \text{ nm}$ of the ligand (Figure 3c and Table 1) indicates that the effects of the ligand on water mobility are mainly limited to the first solvation shell, although a slight slowdown is still found in the second solvation shell at $\xi = 1.15$ nm. This implies that the ligand disrupts the rearrangements of the hydrogen-bond network at a local level, with molecules in the second solvation shell effectively experiencing the same dynamics as in the bulk.

Since the vibrational stretching frequencies of the water molecules are extremely sensitive to the surrounding environment,²⁸ a direct connection between the structural and dynamical properties of the hydration shells around the ligand at different stages of the binding process can be obtained from the analysis of linear and nonlinear IR spectra. The OD lineshapes calculated using eq 1 including all molecules within 0.8 nm of the ligand at $\xi = 1.15$, 0.40, and -0.35 nm are shown

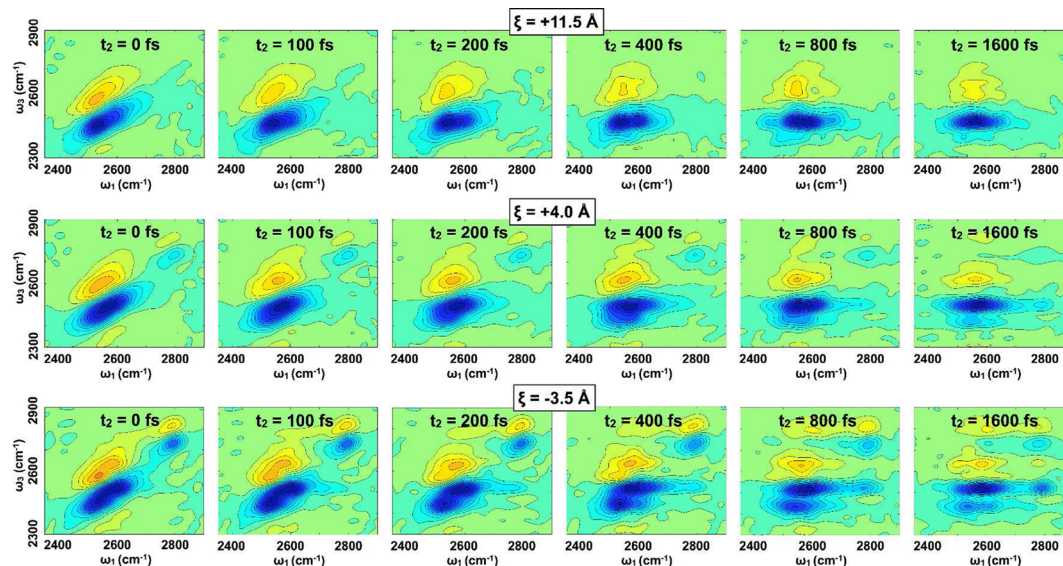


Figure 7. Time evolution of the two-dimensional infrared spectra (2D-IR) calculated from molecular dynamics simulations at the key stages along the cavity–ligand binding coordinate, ξ , as in Figure 1 ($\xi = 1.15$ nm; $\xi = 0.40$ nm, red lines; $\xi = -0.35$ nm). See section 2 for computational details.

in Figure 4. Also shown for reference is the corresponding OD line shape obtained for the bulk HOD:H₂O system.^{38,40} When the ligand is far from the cavity, the lineshape associated with molecules within the first two solvation shells is qualitatively similar to that obtained for bulk water, suggesting a similar hydration structure. As the ligand approaches the cavity, a shoulder at high frequencies appears, which becomes a well-defined secondary peak (~ 2680 cm⁻¹) when the ligand is inside the cavity. It should also be noted that, at $\xi = -0.35$ nm, a small shoulder appears at ~ 2500 cm⁻¹. To characterize the underlying water structure associated with the evolution of the IR lineshape as the ligand approaches the cavity, the occurrence of different topologies of H-bond configurations was investigated from analysis of the corresponding contributions to the IR stretch band. Following ref 45, the frequency distributions corresponding to the IR lineshapes of Figure 4 were decomposed based on possible H-bond configurations of the HOD molecule. In this study, a common geometric definition of hydrogen bonds is employed according to which hydrogen bond is established between two water molecules when the distance between the donor (O_d) and acceptor (O_a) oxygen atoms is $R_{\text{OdOa}} < 3.5$ Å and the hydrogen-bond angle ($\beta = \text{H}_d-\text{O}_d\cdots\text{O}_a$) is $\beta < 30^\circ$. Each H-bond configuration is described in terms of the number of H-bonds involving the O atom (n_O), the D atom (n_D), and the H atoms (n_H) of the HOD molecule. Eight different classes are defined here according to the triplet of numbers N_O , N_D , and N_H . The possible values are $N_O = 1$ corresponding to $n_O = 0, 1$, and $N_O = 2$ corresponding to $n_O = 2, 3$; $N_D = 0$ corresponding to $n_D = 0$, and $N_D = 1$ corresponding to $n_D = 1, 2$; $N_H = 0$ corresponding to $n_H = 0$, and $N_H = 1$ corresponding to $n_H = 1, 2$.

In the following analysis, these classes are labeled according to the total number of H-bonds, the number of H-bond donors, and the D or H label in the case of single donors. Cartoon of the eight possible H-bond topologies are illustrated in Figure 5. Figure 6 shows the frequency distributions associated with both the first (bottom panels) and second (top panels) hydration shells for each of the eight classes along the binding coordinate. Also shown are the corresponding total distributions.

Dissection of the lineshape in terms of the different H-bond typologies indicates that, at $\xi = 1.15$ nm, the water molecules within the first two solvation shells around the ligand are preferentially arranged in a tetrahedral geometry. This can be explained by considering that, due to its relatively small dimensions, the ligand does not affect the overall structure of the H-bond network, which is consequently very similar to that obtained in bulk water.⁴⁰

As the ligand approaches the cavity, less tetrahedral configurations become increasingly important, which is consistent with the appearance of a secondary peak at high frequencies in the OD lineshape. This can be attributed to single donor–single acceptor HOD molecules with dangling O–D bonds. The small shoulder that appears at ~ 2500 cm⁻¹ can instead be attributed to the larger contributions associated with the 2_{SD} and 3_D modes. Importantly, at $\xi = -0.35$ nm, the contribution to the IR lineshape arising from tetrahedral arrangements of water molecules within 0.55 nm of the ligand is small, indicating that the hydration structure becomes significantly different from that observed in the bulk as the ligand approaches the cavity.

Molecular-level information on the water dynamics around the ligand and its relation to the underlying rearrangements of the hydrogen-bond network during the association process can be obtained from analysis of the 2D-IR spectra as a function of the waiting time (t_2), as summarized in Figure 7. At $\xi = 1.15$ nm, the spectra are very similar to those obtained for dilute mixtures of HOD in H₂O.³⁸ Specifically, they are characterized by two peaks, which are elongated along the diagonal at short waiting times, corresponding to the 1–0 (warm colors) and 2–1 (cold colors) resonances. Because of spectral diffusion, the correlation found at short times, which reflects the persistence of memory of the initial OD excitation frequency, is progressively lost as t_2 increases. By contrast, the 2D-IR spectra calculated at both $\xi = 0.40$ and -0.35 nm display some peculiar features. In particular, two additional peaks appear at high frequency along the diagonal at $t_2 = 0$ ps, which correspond to 1–0 and 2–1 transitions associated with nontetrahedral water molecules around the ligand. As t_2 progresses, off-diagonal peaks also appear indicating that the water molecules change

local environments on a time scale of \sim 100 fs, with molecules initially absorbing at high frequency found at lower frequency at later times. These spectroscopic features are directly connected to the faster orientational dynamics observed for water molecules around the ligand as the latter approaches the cavity.

4. CONCLUSIONS

We characterized hydrophobic cavity–ligand association in a model system through the analysis of water structure, dynamics, and corresponding spectral signatures based on MD simulations at different stages of the binding process. The reorientation of the water molecules around the ligand becomes increasingly faster approaching the cavity along the binding coordinate. This dynamic behavior is well correlated with the decrease in number of water–water hydrogen bonds found in the ligand hydration shells.

The simulation results show that the degree of tetrahedrality of water structure around the ligand drops upon binding, indicating that it becomes significantly less favorable for water to hydrate the methane-like ligand with tetrahedral geometries. Similarly, water dynamics speeds up during the dehydration phase of the binding process reflecting the disruption of ligand hydration shell upon transfer to hydrophobic cavity environment. Our data fully supports the thermodynamic analyses for cavity–ligand association previously proposed.^{1,2,46}

The local structure and dynamics of water around a hydrophobic ligand can be directly probed by spectroscopic observables. In the present study, these observables were calculated from simulations. In the future, we suggest that ultrafast vibrational spectroscopy experiments could be used to resolve these spectral signatures. Overall, the present results underscore the importance of integrating computer simulations with vibrational spectroscopy as a route to characterize the molecular mechanisms responsible for molecular recognition and extend these approaches to complex biomolecular systems.

■ AUTHOR INFORMATION

Corresponding Author

*E-mail: r.baron@utah.edu (R.B.); piotr.setny@tum.de (P.S.); fpaesani@ucsd.edu (F.P.).

Present Address

[†]Department of Medicinal Chemistry, College of Pharmacy, and The Henry Eyring Center for Theoretical Chemistry, University of Utah, Salt Lake City, Utah 84112, United States.

Notes

The authors declare no competing financial interest.

■ ACKNOWLEDGMENTS

R.B. acknowledges startup funding from the Department of Medicinal Chemistry, The University of Utah, and technical support from the Center for High Performance Computing. This work used the Extreme Science and Engineering Discovery Environment (XSEDE), which is supported by National Science Foundation grant number OCI-1053575 (allocations TG-CHE120034 and TG-CHE120086 to R.B., and TG-CHE110009 to F.P.). This research was supported in part by the National Science Foundation through grant CHE-1038028 (CCI Center for Aerosol Impacts on Climate and the Environment) to F.P. P.S. is supported by DFG(SFB1035) from Germany.

■ REFERENCES

- (1) Baron, R.; Setny, P.; McCammon, J. A. *J. Am. Chem. Soc.* **2010**, *132*, 12091.
- (2) Setny, P.; Baron, R.; McCammon, J. A. *J. Chem. Theory Comput.* **2010**, *6*, 2866.
- (3) Hummer, G. *Nat. Chem.* **2010**, *2*, 906.
- (4) Baron, R.; McCammon, J. A. *Annu. Rev. Phys. Chem.* **2013**, in press.
- (5) Denisov, V. P.; Venu, K.; Peters, J.; Horlein, H. D.; Halle, B. *J. Phys. Chem. B* **1997**, *101*, 9380.
- (6) Englert, L.; Biela, A.; Zayed, M.; Heine, A.; Hangauer, D.; Klebe, G. *Biochim. Biophys. Acta* **2010**, *1800*, 1192.
- (7) Baron, R.; Setny, P.; McCammon, J. A. Hydrophobic Association and Vol.-Confined Water Molecules. In *Protein-Ligand Interactions*; Gohlke, H., Ed.; Wiley-VCH: Weinheim, Germany, 2011; p 145.
- (8) Abel, R.; Young, T.; Farid, R.; Berne, B. J.; Friesner, R. A. *J. Am. Chem. Soc.* **2008**, *130*, 2817.
- (9) Michel, J.; Tirado-Rives, J.; Jorgensen, W. L. *J. Am. Chem. Soc.* **2009**, *131*, 15403.
- (10) van der Spoel, D.; van Maaren, P. J.; Larsson, P.; Timneau, N. *J. Phys. Chem. B* **2006**, *110*, 4393.
- (11) Setny, P.; Geller, M. *J. Chem. Phys.* **2006**, *125*, 144717.
- (12) Setny, P. *J. Chem. Phys.* **2007**, *127*, 054505.
- (13) Setny, P. *J. Chem. Phys.* **2008**, *128*, 125105.
- (14) Zangi, R.; Berne, B. J. *J. Phys. Chem. B* **2008**, *112*, 8634.
- (15) Chandler, D. *Nature* **2005**, *437*, 640.
- (16) Berne, B. J.; Weeks, J. D.; Zhou, R. H. *Annu. Rev. Phys. Chem.* **2009**, *60*, 85.
- (17) Giovambattista, N.; Lopez, C. F.; Rossky, P. J.; Debenedetti, P. G. *Proc. Natl. Acad. Sci. U.S.A.* **2008**, *105*, 2274.
- (18) Liu, P.; Huang, X. H.; Zhou, R. H.; Berne, B. J. *Nature* **2005**, *437*, 159.
- (19) Mittal, J.; Hummer, G. *Proc. Natl. Acad. Sci. U.S.A.* **2008**, *105*, 20130.
- (20) Rasaiah, J. C.; Garde, S.; Hummer, G. *Annu. Rev. Phys. Chem.* **2008**, *59*, 713.
- (21) Rowlinson, J. S.; Widom, B. *Molecular Theory of Capillarity*; Oxford University Press: New York, 1989.
- (22) Yin, H.; Hummer, G.; Rasaiah, J. C. *J. Am. Chem. Soc.* **2007**, *129*, 7369.
- (23) Dunitz, J. *Science* **1994**, *264*, 670.
- (24) Homans, S. W. *Drug Discovery Today* **2007**, *12*, 534.
- (25) Barratt, E.; Bingham, R. J.; Warner, D. J.; Laughton, C. A.; Phillips, S. E. V.; Homans, S. W. *J. Am. Chem. Soc.* **2005**, *127*, 11827.
- (26) Leung, D. H.; Bergman, R. G.; Raymond, K. N. *J. Am. Chem. Soc.* **2008**, *130*, 2798.
- (27) Fadda, E.; Woods, R. *J. Chem. Theory Comput.* **2011**, *7*, 3391.
- (28) Bakker, H. J.; Skinner, J. L. *Chem. Rev.* **2010**, *110*, 1498.
- (29) Fayer, M. D. *Annu. Rev. Phys. Chem.* **2009**, *60*, 21.
- (30) Roberts, S. T.; Ramasesha, K.; Tokmakoff, A. *Acc. Chem. Res.* **2009**, *42*, 1239.
- (31) Jorgensen, W. L.; Chandrasekhar, J.; Madura, J. D.; Impey, R. W.; Klein, M. L. *J. Chem. Phys.* **1983**, *79*, 926.
- (32) Jorgensen, W. L.; Madura, J. D.; Swenson, C. J. *J. Am. Chem. Soc.* **1984**, *106*, 6638.
- (33) Baron, R.; Molinero, V. *J. Chem. Theory Comput.* **2012**, *8*, 3696.
- (34) Brooks, B. R.; Brooks, C. L., III; Mackerell, A. D., Jr.; Nilsson, L.; Petrella, R. J.; Roux, B.; Won, Y.; Archontis, G.; Bartels, C.; Boresch, S.; Caflisch, A.; Caves, L.; Cui, Q.; Dinner, A. R.; Feig, M.; Fischer, S.; Gao, J.; Hodoscek, M.; Im, W.; Kuczera, K.; Lazaridis, T.; Ma, J.; Ovchinnikov, V.; Paci, E.; Pastor, R. W.; Post, C. B.; Pu, J. Z.; Schaefer, M.; Tidor, B.; Venable, R. M.; Woodcock, H. L.; Wu, X.; Yang, W.; York, D. M.; Karplus, M. *J. Comput. Chem.* **2009**, *30*, 1545.
- (35) Ryckaert, J.-P.; Ciccotti, G.; Berendsen, H. J. C. *J. Comput. Phys.* **1977**, *23*, 327.
- (36) Mukamel, S. *Principles of Nonlinear Optical Spectroscopy*; Oxford University Press: New York, 1995.
- (37) Numerov, B. V. *Mon. Not. R. Astron. Soc.* **1924**, *84*, 592.
- (38) Paesani, F. *J. Phys. Chem. A* **2011**, *115*, 6861.

- (39) Paesani, F. *Phys. Chem. Chem. Phys.* **2011**, *13*, 19865.
(40) Paesani, F.; Xantheas, S. S.; Voth, G. A. *J. Phys. Chem. B* **2009**, *113*, 13118.
(41) Fanourgakis, G. S.; Xantheas, S. S. *J. Chem. Phys.* **2008**, *128*, 074506.
(42) Paesani, F.; Yoo, S.; Bakker, H. J.; Xantheas, S. S. *J. Phys. Chem. Lett.* **2010**, *1*, 2316.
(43) Rezus, Y. L. A.; Bakker, H. J. *Phys. Rev. Lett.* **2007**, *99*, 148301.
(44) Laage, D.; Stirnemann, G.; Hynes, J. T. *J. Phys. Chem. B* **2009**, *113*, 2428.
(45) Auer, B.; Kumar, R.; Schmidt, J. R.; Skinner, J. L. *Proc. Natl. Acad. Sci. U.S.A.* **2007**, *104*, 14215.
(46) Setny, P.; Baron, R.; McCammon, J. A. *Chem. Phys. Lett.* **2012**, in press.